Electronic Implants: Power Delivery and Management

Jacopo Olivo, Sara S. Ghoreishizadeh, Sandro Carrara, and Giovanni De Micheli
Integrated Systems Laboratory - EPFL
Lausanne, Switzerland
email: jacopo.olivo@epfl.ch

Abstract—A power delivery system for implantable biosensors is presented. The system, embedded into a skin patch and located directly over the implantation area, is able to transfer up to 15 mW wirelessly through the body tissues by means of an inductive link. The inductive link is also used to achieve bidirectional data communication with the implanted device. Downlink communication (ASK) is performed at 100 kbps; uplink communication (LSK) is performed at 66.6 kbps. The received power is managed by an integrated system including a voltage rectifier, an amplitude demodulator and a load modulator. The power management system is presented and evaluated by means of simulations.

Index Terms—Remote powering, inductive link, energy harvesting, implantable biosensors, lactate measurement.

I. INTRODUCTION

The research field of implantable biosensors has attracted the interest of academia and industry in the last two decades. The possibility of continuous monitoring of the human body from inside is an opportunity to better understand the ways the body works and paves the way to a large number of applications.

As an example, the continuous monitoring of the glucose level in the subcutaneous interstitial fluids is an important aid to those patients who suffer from diabetes. By using implantable sensors located in the subcutaneous zones, the percentage of glucose in the blood (*glycemia*) can be recorded and analyzed [1]. Thus, periodic and disturbing blood sampling can be avoided. Lactate can also be monitored by means of subcutaneous sensors [2]. The lactate concentration in the blood (*lactatemia*) or interstitial tissues in muscle can be recorded to monitor the muscular effort in sportsmen or people under rehabilitation. Finally, many other human metabolites can be detected with subcutaneous biosensors [3].

Several key challenges must be addressed to realize these scenarios [4]: implantable biosensors should be minimally invasive, completely biocompatible, highly reliable, and with a low thermal dissipation. Security and privacy should be provided during data transmission. Finally, large power autonomy should be ensured. This last requirement must be carefully

considered, since the performance and the invasivity of an implantable sensor strongly depend by the battery size and the battery lifetime.

Modern batteries have increased capabilities with respect to those available in the past. As an example, lithium-ion batteries have reached a high level of energy density (up to $0.2\,\mathrm{Wh/g}$) and can maintain an almost constant voltage until they are discharged to 75%-80% [5]. Furthermore, thin-film rechargeable batteries can sensibly reduce the size of battery-powered devices [6]. However, even with an improved energy density, batteries still represent a bottleneck in the miniaturization of implantable sensors. Moreover, substituting the battery can cause discomfort to the patient.

Energy harvesting techniques exploit natural and/or artificial power sources surrounding the person to assist the implanted batteries, to recharge them and in certain cases replace them. A review of the most popular harvesting techniques for implantable sensor can be found in [7].

Remote powering through inductive link is a well known method of delivering power to an implanted device. In such a technique, a current flowing through an external inductor (*transmitter*) induces a current through one or more implanted inductors (*receiver*); thus, power is transmitted wirelessly through the body tissues. Several solutions have been proposed in the literature [8–17]. Commercial devices exploiting inductive links for the remote powering of implantable systems already reached the market [18]. However, the wearability of the power transmitter (delivery module) and the miniaturization of the implanted receiver (delivery and management modules) is still an open research topic.

Inductive links are also used to perform bidirectional data communication with the implanted devices [8, 12, 13, 15]. Downlink communication (from the external transmitter to the implanted device) can be obtained by modulating the power carrier generated by the transmitter. Uplink communication (from the implanted device to the external transmitter) can be obtained by modulating the load of the receiving inductor; this modulation is detected as a change of current flowing through the external inductor. Thus, no implanted RF transmitter is needed.

The focus of this paper is on the power delivery and power management. A target device for metabolite measurement is reported in Section II. Section III describes the system
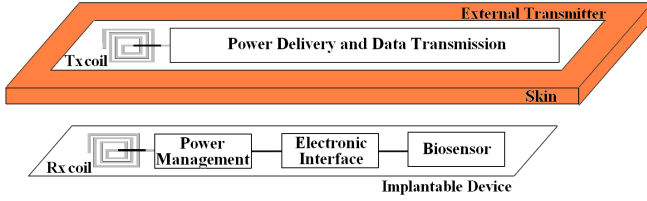
Fig. 1. Schematic view of the implantable system and the power delivery module.

Fig. 2. Three-electrode electrochemical cell and measurement set-up.

designed to remotely power the target device. The electronics to manage the received power and to efficiently store it is presented in Section IV. Finally, Section V concludes the paper.

II. TARGET DEVICE

A. System Description

In this section a metabolite sensor and the integrated circuit to perform metabolite measurements are presented. A diagram of the system is shown in Fig. 1. The main blocks of the implantable device are the biosensor, the electronic interface, the power management module, and the receiving inductor.

The biosensor consists of an electrochemical cell with three electrodes (Fig. 2). In order to measure the metabolite concentration, a fixed voltage V_{ox} (oxidation potential) is applied between *working electrode* (WE) and *reference electrode* (RE). As a result, a current flows between the working electrode and the *counter electrode* (CE) due to the metabolite oxidation. To increase the biosensor selectivity to a specific target, different enzymes can be immobilized on the surface of the working electrode [19].

A main issue of metabolite biosensors is the lack of stability. Moreover, the sensor parameters are strongly affected by the immobilization method of the enzyme onto the electrode. Previous works have investigated the use of *multi-walled carbon nanotubes* (MWCNTs) to immobilize the enzyme onto the electrodes [20, 21]. The enhanced adhesion, due to MWCNTs, improves the performance of the sensor [20].

B. Circuit Design

An *electronic interface* (EI) is designed to perform electrochemical measurements of lactate with the three-electrode configuration of Fig. 2. The EI, reported in Fig. 3, includes the potentiostat, the readout circuit, the reference voltage generators and the ADC.

The potentiostat consists of OPAMPs OP_1 and OP_2, together with transistors MP_0 and MP_2. It applies a fixed voltage of $650\,\mathrm{mV}$ (oxidation potential of several metabolites, including glucose and lactate) between WE and RE.

The readout circuit consists of current mirrors and a resistor to generate a copy of the cell current I_{WE}. The copied current is then converted into a voltage and measured, while providing isolation for the sensor current I_{WE}. The potentiostat and the readout circuit are fabricated in $0.18\,\mathrm{\mu m}$ CMOS technology and consume $45\,\mathrm{\mu A}$ with a supply voltage of $1.8\,\mathrm{V}$.
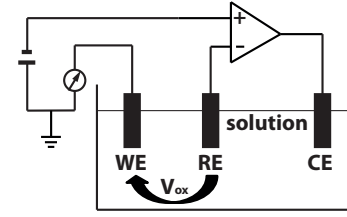

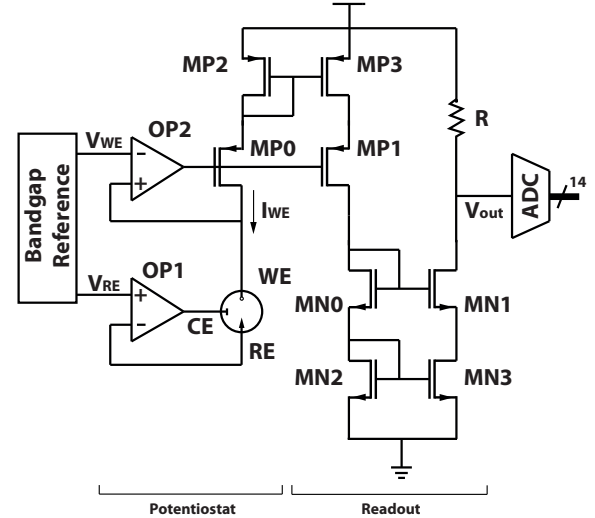Fig. 3. Electronic interface for metabolite measurement.

Two bandgap reference circuits are designed to generate a voltage of $650\,\mathrm{mV}$ between WE and RE. That voltage is independent from temperature and supply. A voltage of $550\,\mathrm{mV}$ is applied to the RE by means of a sub-1V bandgap reference [22]; a voltage of $1.2\,\mathrm{V}$ is applied to the WE by means of a regular bandgap reference. Thus, $650\,\mathrm{mV}$ are measured between WE and RE.

An ADC is designed to digitize the output voltage of the readout circuit. The current range and the sensitivity of the biosensor depends on the geometry of the electrodes and the enzyme used [3, 21]. In this work, the maximum value of I_{WE} is set to $4\,\mathrm{\mu A}$ and the current resolution is set to $250\,\mathrm{pA}$, in order to be compliant with a wide range of sensors with different geometries and enzymes. To digitize $4\,\mathrm{\mu A}$ with the resolution of $250\,\mathrm{pA}$, a 14-bit ADC is required. The designed ADC is a second order sigma-delta, implemented in $0.18\,\mathrm{\mu m}$ CMOS technology. The area of the ADC and the bandgap reference is $0.3\,\mathrm{mm^2}$. The simulated current consumption is $240\,\mathrm{\mu A}$ with a supply voltage of $1.8\,\mathrm{V}$.

C. Measurement Results

The potentiostat and the readout circuit in Fig. 3 are used to measure lactate concentration. Two different enzymes are immobilized on the screen printed electrodes: commercial (cLODx) and wild type (wtLODx). MWCNTs are used to enhance the performance of the sensor. The measured char-
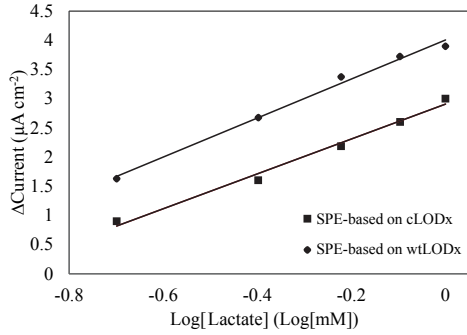
Fig. 4. Lactate measurement using the potentiostat and the readout circuit reported in Fig. 3.
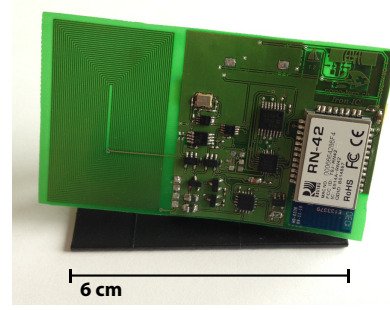

Fig. 5. The IronIC patch can be placed over the implantation zones, in concave or convex parts of the body, to power implanted sensors and communicate with them.

acteristic is shown in Fig. 4. The results are in agreement with those obtained with a commercial potentiostat. A detailed discussion can be found in [23].

III. POWER DELIVERY

In this section is described the device to deliver power to the target sensor presented in Section II. Further details can be found in [24]. The system, named IronIC patch, is designed to be embedded into a skin patch and placed directly over the implantation zones. Designed on a flexible substrate, the device can be used on concave or convex parts of the body (Fig. 5).

A. System Description

A schematic description of the patch is given in Fig. 6, from [24]. Power is transmitted to the implanted system by driving the transmitting inductor with a class-E power amplifier. Amplifiers in class-E are commonly used to drive inductive links due to the high efficiency, theoretically equal to 100% [25–27]. Indeed, by properly tuning the amplifier capacitors C_3 and C_4, the current and the voltage across the switch M_2 are never non-zero at the same time. In this design, the amplifier is driven by a 5 MHz square waveform with duty cycle 50%.

Downlink communication is achieved by modulating the amplitude of the current flowing on the transmitting inductor L_2. Amplitude modulation (*Amplitude Shift Keying* - ASK) is a common approach when no high data-rates are required. Indeed, it noticeably simplifies the design of the embedded demodulator. The modulating signal is a bitstream generated by the microcontroller. The bit-rate is set to 100 kbps. Modulation depth is determined by the ratio between resistors R_7 and R_8.

Uplink communication is achieved by modulating the load of the receiving inductor and detecting that modulation on the supply current of the class-E amplifier (*Load Shift Keying* - LSK). To demodulate an uplink bitstream, the voltage drop across R_9 is digitized and analyzed by the microcontroller. A high voltage drop, due to a high current, is detected when the receiving inductor is not short-circuited; a low voltage drop, due to a low current, is detected when the receiving inductor
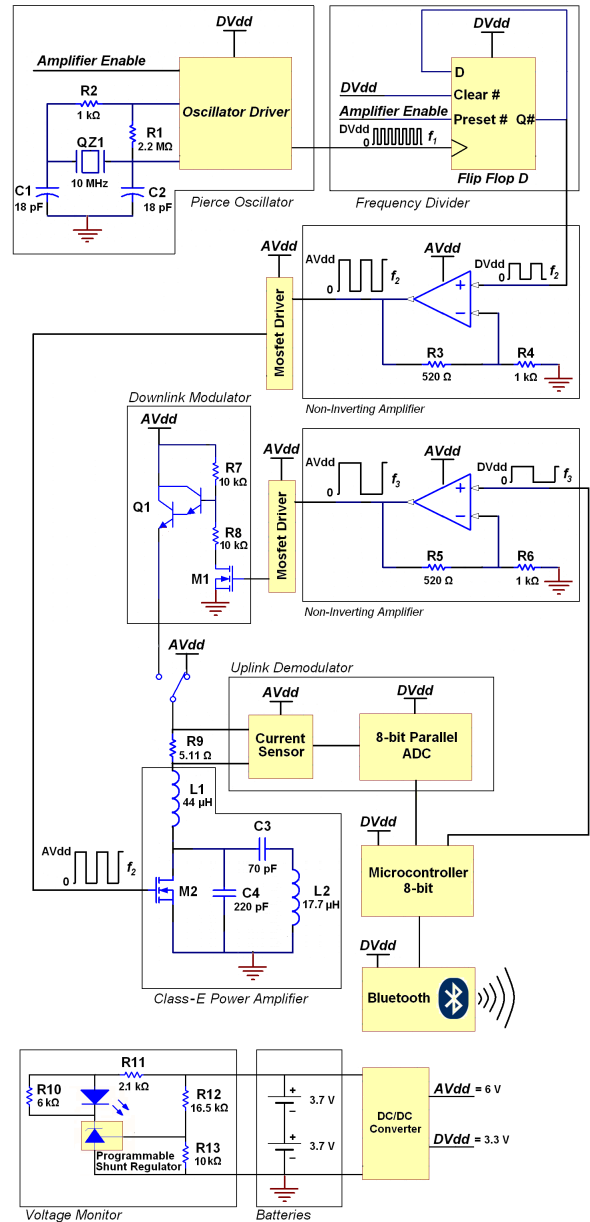

Fig. 6. Schematic of the IronIC patch at component level. Reprinted from [24].
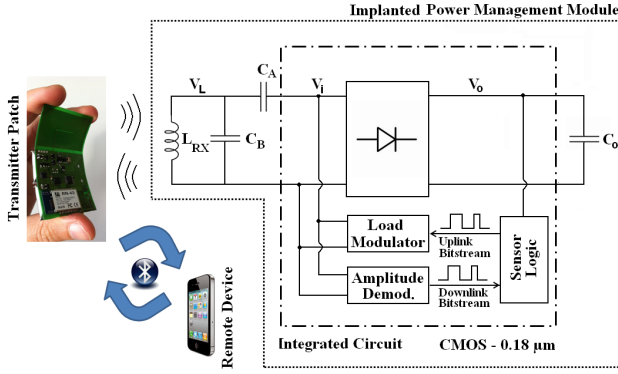
Fig. 7. The implanted sensor receives power and data from the external device (transmitter patch). The transmitter performs long-range communication with remote devices by means of bluetooth.

Fig. 8. Schematic of the voltage rectifier and the load modulation unit.

is short-circuited. Uplink bit-rate is set to 66.6 kbps. This value is slightly lower than the downlink bit-rate due to the computational time required to perform a real-time threshold check between high and low current values.

The whole system (amplifier, modulator, and demodulator) can be driven by a remote device, such as a laptop or a smartphone, by means of bluetooth connection. Moreover, acquired data are transmitted to the user by means of the bluetooth link.

B. System Performance

The system described is tested in air by using an 8-layer, 14-turn receiving inductor, having volume $38 \times 2 \times 0.544$ mm^3 [24]. Further details on the fabrication of the receiving inductor can be found in [28].

The received power, within a distance of 6 mm between the inductors, is 15 mW. This value corresponds to the maximum transmitted power. The transmitted power can be decreased by properly tuning the class-E amplifier if a lower value is required by the implantable sensor. Measurements have been performed by using a beef sirloin between the inductors to emulate the presence of biological tissues. While a 17 mm thick slice of sirloin is placed between the coils, the transferred power is 1.17 mW. This value is similar to that obtained in air, where the distance between the coils is set to 17 mm.

While the patch is disconnected by the bluetooth and it is not sending power, the estimated battery duration is about 10 h. This value decreases when the system is connected to a remote device, such as a laptop or a smartphone. In that case, the estimated battery duration is about 3.5 h. While disconnected from the bluetooth, the patch can send power continuously for 1.5 h.

IV. Power Management

In order to use the power delivered by the receiving inductor, the implantable sensor must be equipped with a voltage rectifier and a low-dropout regulator. Moreover, an amplitude demodulator and a load modulator are needed to enable the downlink and the uplink communications, respectively. These circuits (rectifier, regulator, amplitude demodulator, and load
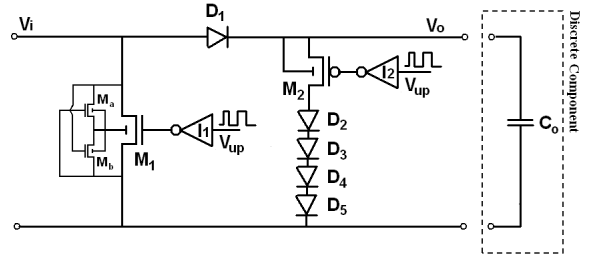
modulator) should be integrated within the sensor to provide a stable supply voltage and perform bidirectional, short-range communication.

In this section we describe the design of a power management module including voltage rectifier, ASK demodulator and LSK modulator. The module is designed in 0.18 μm CMOS technology. A schematic view of the power management module is shown in Fig. 7.

A. Voltage Rectifier and Load Modulator

The schematic of the voltage rectifier is reported in Fig. 8, together with the load modulation unit. At the beginning of the operations, when no power is transmitted and the output capacitor is discharged, switch M_1 is open and switch M_2 is closed. Thus, the equivalent circuit is an half-wave rectifier with four clamping diodes to prevent overvoltage of the output ($V_o \leq 3$ V). That configuration remains unchanged when capacitor C_o is charged and a stable supply voltage is provided on-chip.

Load modulation is performed by switching the transistor M_1 at the input of the rectifier according to the uplink bitstream V_{up}. When a low logic value is transmitted, the switch M_1 is closed and short-circuits the input of the rectifier; thus, no power is delivered to the load. To avoid the discharge of C_o due to the leakage current of the clamping diodes, switch M_2 is kept open when a low logic value is transmitted.

To prevent the latch-up of M_1 when the input voltage V_i has negative values, its bulk is not connected to ground. Transistor M_a and M_b are used to bias the bulk of M_1 to the lowest between drain and source voltages. To realize such circuit, the bulks of M_1, M_a, and M_b are fabricated within a separate n-well (triple well).

B. Amplitude Demodulator

As previously said, the power management module is equipped with an embedded ASK demodulator to read downlink bitstreams transmitted by the external patch. The schematic of the demodulator is reported in Fig. 9.

The circuit is driven by a two-phase non-overlapping clock signal (φ_1 and φ_2, in Fig. 9). While signal φ_1 is high, the equivalent circuit is the one reported in Fig. 10a. Capacitor C_2 is charged to the amplitude of the sinusoidal signal V_i through the switch M_{10}. Diodes D_6, D_7 and D_8 prevent the discharge. The voltage across C_2 is read as a logic value by inverters I_3 and I_4. During this phase, capacitor C_1 is discharged.
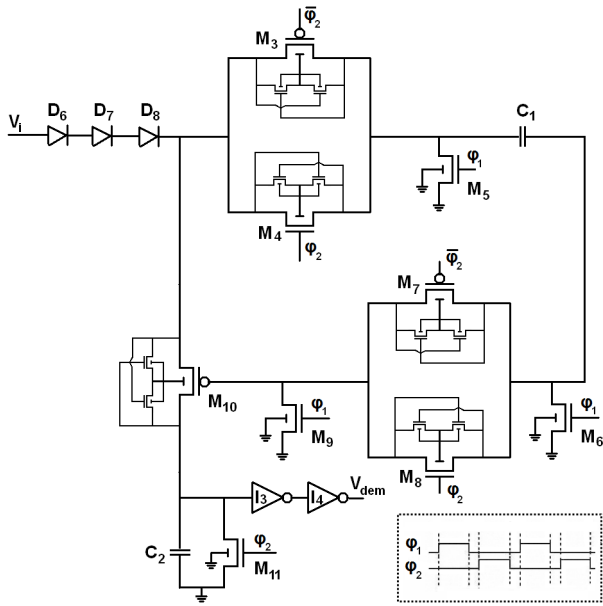
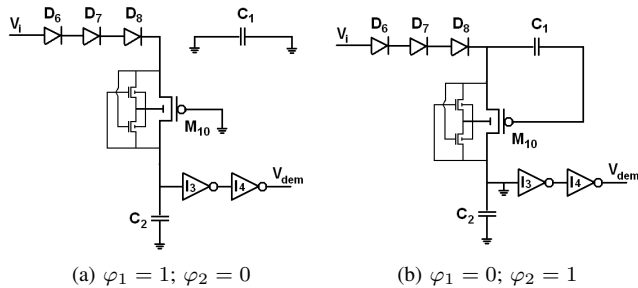Fig. 9. Schematic of the amplitude demodulator. The circuit is driven by a two-phase non overlapping clock signal (φ_1 and φ_2).

(a) $\varphi_1 = 1$; $\varphi_2 = 0$ (b) $\varphi_1 = 0$; $\varphi_2 = 1$

Fig. 10. Equivalent circuit of the demodulator in Fig. 9 while $\varphi_1 = 1$ (a) and $\varphi_2 = 1$ (b).

When signal φ_2 is high, the equivalent circuit is the one reported in Fig. 10b. Capacitor C_1, previously discharged, forces a zero voltage between gate and source of M_{10}. Thus, switch M_{10} is open disregarding the value of V_i. During this phase, capacitor C_2 is discharged and the output of inverters I_3 and I_4 is neglected.

Similarly to what happens with transistor M_1 of the rectifier (Fig. 8), a sub-circuit is included to bias the bulk of M_{10} and prevent latch-up.

C. Simulations

The power management module is simulated to check the performance. While receiving or transmitting a bitstream, the sensor is assumed in low power mode, with a maximum current consumption of about 350 μA; while performing a measurement, the sensor is assumed in high power mode, with a maximum current consumption of about 1.3 mA. These power consumptions are much higher than those previously reported. However, a worst scenario is assumed to check the capability of the power module to operate with more power-demanding sensors. In this set of simulations the power

delivered from the receiving inductor to a matched load is equal to 5 mW. This value decreases while downlink communication is performed. While transmitting a high logic value the transferred power is about 3 mW; while transmitting a low logic value the transferred power is about 1 mW. These values have been measured with the external patch described in Section III within a distance of 10 mm between the inductors.

A purely capacitive matching network (C_A and C_B in Fig. 7) is used between the receiving inductor and the input of the rectifier to have impedance matching. Due to the non-linearity of the rectifier, it is not possible to define a linear input impedance for that block. Thus, simulations have been performed to determine an average value for the input impedance of the rectifier. With the data just introduced, the average input impedance of the rectifier is about 150 Ω. This value is used to select capacitors C_A and C_B of the matching network.

By considering the dropout voltage of the regulator equal to 300 mV, the output voltage V_o of the rectifier should always be higher than 2.1 V to assure the correct functioning of the sensor at 1.8 V. A simulation is performed to check the behavior of the rectifier and the amplitude demodulator (Fig. 11).

Capacitor C_o is charged until it reaches a voltage of 2.75 V at time 270 μs. Eighteen bits, with a bit-rate of 100 kbps, are sent to the sensor by modulating the signal V_i at time 300 μs. Those bits are correctly detected at the output V_{dem} of the demodulator at every rising edge of the clock signal φ_1. During the communication, the output voltage V_o of the rectifier never goes below 2.1 V. An uplink communication is simulated at time 520 μs. Several bits are sent with a bit-rate of 100 kbps from the sensor to the external patch by short-circuiting the input of the rectifier, according to signal V_{up} of Fig. 8. The effect of such modulation on the input voltage V_i is reported in Fig. 11. Similarly to what reported for the downlink communication, the output voltage V_o of the rectifier never goes below 2.1 V during the transmission.

V. CONCLUSIONS

A power delivery system for implantable sensors is presented. Power delivery and power management modules are reported, together with a description of the implantable sensor to be powered.

An external delivery device, embedded into a skin patch, is able to transmit up to 15 mW through inductive link, within a distance of 6 mm between the transmitting and the receiving inductors. Downlink communication is performed at 100 kbps with ASK modulation; uplink communication is performed at 66 kbps with LSK modulation. Long range communication with a remote device is enabled by a bluetooth module embedded into the patch.

The power management module, including voltage rectifier, amplitude demodulator, and load modulator is presented and discussed by means of simulations. The design has been fabricated in 0.18 μm CMOS technology. Future works will involve the circuit characterization by means of measurements.
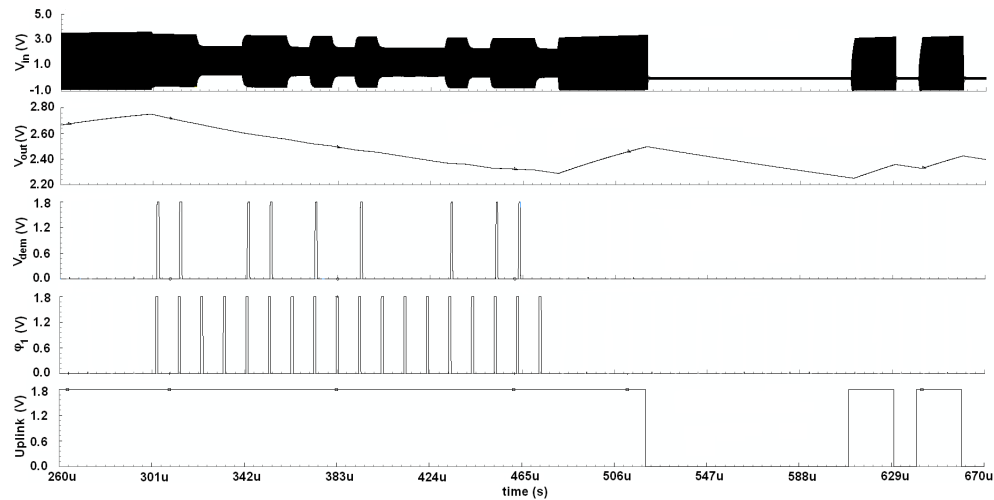
Fig. 11. The power module is simulated to check the performance. Downlink and uplink communications are correctly performed at 100 kbps. The output of the rectifier is always higher than 2.1 V; thus, the regulator can provide a stable supply voltage of 1.8 V to the sensor.

VI. Acknowledgement

References

[1] F. Valgimigli, F. Lucarelli, C. Scuffi, S. Morandi, and I. Sposato, "Evaluating the Clinical Accuracy of GlucoMen Day: A Novel Microdialysis-based Continuous Glucose Monitor," *J Diabetes Sci Technol.*, vol. 4, p. 11821192, 2010.

[2] A. Poscia, D. Messeri, D. Moscone, F. Ricci, and F. Valgimigli, "A Novel Continuous Subcutaneous Lactate Monitoring System," *Biosens Bioelectron*, vol. 20, pp. 2244 – 2250, 2005.

[3] G. De Micheli, S. Ghoreishizadeh, C. Boero, F. Valgimigli, and S. Carrara, "An Integrated Platform for Advanced Diagnostics," in *IEEE DATE Conf.*, 2011, pp. 1–6.

[4] S. Carrara, S. Ghoreishizadeh, J. Olivo, I. Taurino, C. Baj-Rossi, A. Cavallini, M. Op de Beeck, C. Dehollain, W. Burleson, F. Moussy, A. Guiseppi-Elie, and G. De Micheli, "Fully Integrated Biochip Platforms for Advanced Healthcare," *Sensors*, vol. 12, pp. 11 013–11 060, 2012.

[5] A. Du Pasquier, I. Plitz, S. Menocal, and G. Amatucci, "A Comparative Study of Li-ion Battery, Supercapacitor and Nonaqueous Asymmetric Hybrid Devices for Automotive Applications," *J. Power Sources*, vol. 115, no. 1, pp. 171–178, Mar. 2003.

[6] Thinergy micro-energy cells (mecs). [Online]. Available: http://www.infinitepowersolutions.com

[7] J. Olivo, S. Carrara, and G. De Micheli, "Energy Harvesting and Remote Powering for Implantable Biosensors," *IEEE Sens. J.*, vol. 11, no. 7, pp. 1573–1586, 2010.

[8] T. Akin, K. Najafi, and R. Bradley, "A Wireless Implantable Multichannel Digital Neural Recording System for a Micromachined Sieve Electrode," *IEEE J. Solid-St. Circ.*, vol. 33, pp. 109 –118, 1998.

[9] C. Sauer, M. Stanaćević, G. Cauwenberghs, and N. Thakor, "Power Harvesting and Telemetry in CMOS for Implanted Devices," *IEEE Trans. Circuits Syst. I, Reg. Papers*, vol. 52, pp. 2605 – 2613, 2005.

[10] B. Lenaerts and R. Puers, "An Inductive Power Link for a Wireless Endoscope," *Biosens Bioelectron*, vol. 22, pp. 1390 – 1395, 2007.

[11] K. Silay, D. Dondi, L. Larcher, M. Declercq, L. Benini, Y. Leblebici, and C. Dehollain, "Load Optimization of an Inductive Power Link for Remote Powering of Biomedical Implants," in *IEEE ISCAS Conf.*, 2009, pp. 533 –536.

[12] M. Catrysse, B. Hermans, and R. Puers, "An Inductive Power System with Integrated Bi-directional Data-transmission," *Sensor Actuat A-Phys*, vol. 115, pp. 221 – 229, 2004.

[13] J. Parramon, P. Doguet, D. Marin, M. Verleyssen, R. Muñoz, L. Leija, and E. Valderrama, "ASIC-Based Batteryless Implantable Telemetry Microsystem for Recording Purposes," *IEEE EMBC*, vol. 5, pp. 2225 –2228, 1997.

[14] G. Gudnason, E. Bruun, and M. Haugland, "A Chip for an Implantable Neural Stimulator," *Analog Integr. Circuits Signal Process.*, vol. 22, pp. 81–89, 2000.

[15] B. Smith, Z. Tang, M. Johnson, S. Pourmehdi, M. Gazdik, J. Buckett, and P. Peckham, "An Externally Powered, Multichannel, Implantable Stimulator-telemeter for Control of Paralyzed Muscle," *IEEE Trans Biomed Eng*, vol. 45, pp. 463 –475, 1998.

[16] M. Ahmadi and G. Jullien, "A Wireless-implantable Microsystem for Continuous Blood Glucose Monitoring," *IEEE Trans. Biomed. Circuits Syst.*, vol. 3, pp. 169 –180, 2009.

[17] S. O'Driscoll, A. Poon, and T. Meng, "A mm-sized Implantable Power Receiver with Adaptative Link Compensation," in *ISSCC - Digest of Technical Papers*, 2009, pp. 294–295, 295a.

[18] Activa RC Recharging System 37751. Medtronic.

[19] I. Taurino, R. Reiss, M. Ritcher, M. Fairhead, L. Thony-Meyer, G. De Micheli, and S. Carrara, "Comparative Study of Three Lactate Oxidases from Aerococcus Viridans for Biosensing Applications," *Electrochim Acta*, in Press.

[20] S. Carrara, V. Shumyantseva, A. Archakov, and B. Samorì, "Screen-Printed Electrodes Based on Carbon Nanotubes and Cytochrome P450scc for Highly Sensitive Cholesterol Biosensors," *Biosens Bioelectron*, vol. 24, pp. 148–150, 2008.

[21] C. Boero, J. Olivo, S. Carrara, and G. De Micheli, "New Approaches for Carbon Nanotubes-Based Biosensors and their Application to Cell Culture Monitoring," *IEEE Trans. Biomed. Circuits Syst.*, in Press.

[22] H. Banba, H. Shiga, A. Umezawa, T. Miyaba, T. Tanzawa, S. Atsumi, and K. Sakui, "A CMOS Bandgap Reference Circuit with Sub-1-V Operation," *IEEE J. Solid-St. Circ.*, vol. 34, pp. 670–674, 1999.

[23] S. Ghoreishizadeh, I. Taurino, S. Carrara, and G. De Micheli, "A Current-Mode Potentiostat for Multi-Target Detection Tested with Different Lactate Biosensors," in *IEEE BioCAS Conf.*, 2012, accepted.

[24] J. Olivo, S. Carrara, and G. De Micheli, "IronIC Patch: A Wearable Device for the Remote Powering and Connectivity of Implantable Systems," in *IEEE I2MTC Conf.*, 2012, pp. 286 – 289.

[25] B. Lenaerts and R. Puers, *Omnidirectional Inductive Powering for Biomedical Implants*. Springer, 2009.

[26] N. Sokal, "Class-E RF Power Amplifiers," *QEX*, pp. 9–20, Jan./Feb. 2001.

[27] F. Raab, "Idealized Operation of the Class-E Tuned Power Amplifier," *IEEE T. Circuits. Syst.*, vol. CAS-24, pp. 725–735, 1977.

[28] J. Olivo, S. Carrara, and G. De Micheli, "A Study of Multi-Layer Spiral Inductors for Remote Powering of Implantable Sensors," *IEEE Trans. Biomed. Circuits Syst.*, in Press.